Chapter 6

Study of multileaf collimator shaped Unflattened photon beam using Monte Carlo Simulations

ABSTRACT

Advancement in equipments and availability of multileaf collimators has removed the essentiality of flattened beam for treatment. The leaf sequences of multileaf collimator (MLC) could be adjusted accordingly to produce desired fluence distributions similar to those achieved with the flattened beam. The present chapter is focused on study of dosimetric properties of unflattened 6 MV photon beam shaped by multileaf collimator and compares them with those of flattened beams using the Monte Carlo (MC) simulations. The BEAMnrc Monte Carlo code was used for making the simulation model of Treatment head of Varian Clinic 600 unique performance linac. This simulation model was used to generate the simulated data for both the flattened and unflattened beam and field sizes were defined using the multileaf collimator instead of X & Y jaws. Dosimetric characteristics including lateral profiles, central axis depth dose, photon and electron fluence spectra were computed for flattened and unflattened beam separately and compared. Our study showed that dosimetric field size and penumbra calculated for unflattened beam were inferior in comparison to the flattened beam, however the decreases in field size were found to be less for MLC shaped unflattened beam in comparison to jaw-shaped unflattened beam. For unflattened beam the MLC leakage calculation showed a significant decrease. Unflattened beam shaped by MLC were found to show least variation in Total scatter factor with respect to change in the field size. Reduced head scatter present in beam will reduce the doses to the normal surrounding organs other then targeted for treatment. Our study demonstrated that improved accelerator characteristics can be achieved with unflattened beam shaped by multileaf collimator.

6.1 INTRODUCTION

Introduction of flattening filter free beams in radiotherapy has generated substantial interest due to the possible advantages offered by the unflattened beams over the flattened beams. Various studies given in the literature have shown that the removal of flattening filter with its associated attenuation from X-ray beam path improves the beam quality **[Fu *et al.* (2004)]**. Medical linear accelerators used for radiotherapy has a flattening filter (FF) as there integral part. The primary intended of flattening filter is to produce a flat beam profile across the field by compensating for the non uniformity of photon fluence. However, the presence of flattening filter produces major quality changes within the primary beam by scattering and absorption of primary photons and it also decreases beam output noticeably. Morden radiotherapy treatments technologies such as intensity modulated radiation therapy (IMRT) uses the Multileaf collimators which are the part of secondary collimator systems of medical linear accelerators to generate an inhomogeneous fluence map eliminating the requirement of uniform initial fluence. Thus flattening filter could be removed from the path of radiation beam which provide other potential benefits such as substantial reduction in head scatter, as the flattening filter is the major source of scattered photons. Improved dosimetry characteristics could also be achieved with a decrease in the variation of all field size dependent parameters. Removal of the flattening filter make changes in the shape of the lateral profiles, the energy spectrum, and increases the dose rate on central axis due to which a decrease in beam-on time can be achieved. Absence of flattening filter reduces the quantity of material present in the path of radiation beam resulting in least amount of out-of–field dose which depends upon the scatter fluence produced by it. Many studies have been carrying out using different Monte Carlo (MC) code systems for analyzing the influence of Treatment head components on beam characteristics **[Verhaegen *et al.* (2003), Sheikh-Bagheri *et al.***

(2002), Mesbahi *et al.* (2006)]. The effect of flattening filter on absolute absorbed dose, beam profiles and various energy spectra have also be studied using these method **[Lee *et al.* (1997)**]. Thus we have used these code systems for our investigation of unflattened beam parameters. The **previous chapter** was focused upon evaluating the dosimetric characteristics of unflattened beam in which the field size were defined using the movable jaws only and did not examine the potential differences between fields shaped by movable jaws and by a MLC for the unflattened beam. To acquire the information of these possible differences, we examined the properties of flattened and unflattened beam in which the treatment fields were shaped by a MLC and then compared them with those for which fields were shaped by jaws only. To accomplish this task, we performed Monte Carlo simulations for computation of lateral profiles, depth dose profiles, MLC leakage, total scatter factors, and various types of fluence spectra.

6.2 Material & Methods

In our study we developed the simulation model of Varian Clinic 600 unique performance linear accelerator using BEAMnrc code System. The entire geometry and materials used to build the MC simulation model of the linear accelerator were based on machine specifications as provided by the manufacturer Varian Medical Systems. The linac was structured in the following order: a target slab of tungsten and copper, primary collimator (tungsten), flattening filter, ion chamber, mirror, jaws (tungsten) and finally the option for 120 leaf Varian Millennium^{TM} Multileaf Collimator. All materials used in the MC simulation were extracted from the 700 ICRU PEGS4 (pre-processor for Electron Gamma Shower) cross-section data available in BEAMnrc. Our simulation model calculations were segmented in three majors steps. Initially $1{\cdot}5\times10^{8}$ histories were used, a monoenergetic electron beam

source of kinetic energy of 5·7 MeV with a full width at half maximum (FWHM) for the X and Y directions of 0·2 cm was made to incident on the target. The primary collimator, flattening filter and ion chamber were included in this step. This step results in a phase space file on the first scoring plane as shown in figure 6.1 containing detailed information of all the particles reaching this plane and there after exiting downstream from the end of ion chamber. This phase space data is reused for the next step of simulation for simulating the particle transport through secondary collimator systems defining different field sizes. The secondary collimator system includes the mirror; adjustable collimator, MLC and air slab up to a plane at source to surface distance (SSD) of 100 cm from target. We simulated different openings of jaw as well as MLC to define field sizes from 5× 5 to 20 × 20 cm^2 at an SSD equal to 100 cm. For the latter case, in MLC defined field sizes the projected jaw setting was 5 cm larger than that of MLC. The secondary phase space file obtained at the scoring plane two was then used to calculate the various types of spectra of all particles reaching at the top of water phantom with the use of data analysis program BEAMDP. Finally this phase space file obtained for different field sizes define by different elements of secondary collimator system are imported as a input inside a water phantom created in DOSXYZnrc code as shown in figure 6.1 for the dose calculations. The water phantom used for the dose calculation was of dimension 30 ×30 × 30 cm^3 with a voxels size of 0·25 × 0·25 × 0·25 cm^3. In the simulation of 'unfiltered' 6MV photon beam, all three steps of simulation were same expect in the first step where the flattening filter was removed from the beam line.

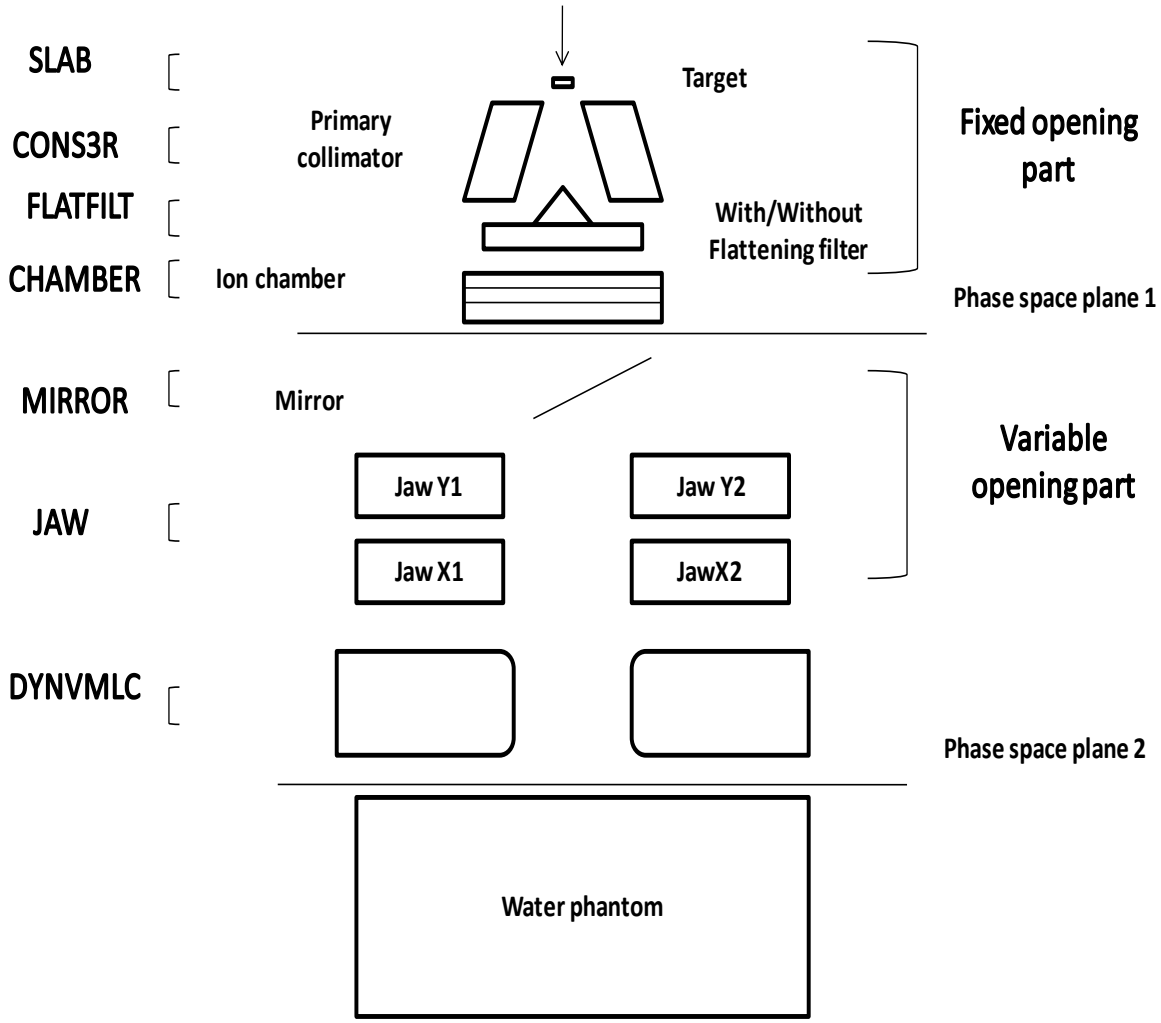

Figure 6.1 Varian Linac simulation model separated into three parts: treatment head fixed Opening part up to scoring plane one, variable opening part between Scoring plane One and two and dose calculation inside the water phantom .

6.3 Analysis of Multileaf collimator Shaped unflattened and flattened beam Characteristics

6.3.1 Profile comparison

In our investigation of unflattened beam delivered after removing the flattening filter from the beam line we used either movable jaws or multileaf collimators to shape the unflattened beam to obtain desired field sizes at source to surface distance of 100 cm. As discussed in the previous chapter that the unflattened beam profile show large quantitative changes with respect to the corresponding flattened beam due to their forward-peaked profile on central axis as shown in figure 6.2. Thus for the lateral beam profile calculated for unflattened beam with Monte Carlo simulation, it was not possible to normalize them with the central axis dose as it is performed for the corresponding flattened beam. We have used two standard methods given in literature whose details we have mentioned in the previous chapter for the profile normalization of unflattened beam so that they can be compared with the flattened beam lateral profile.

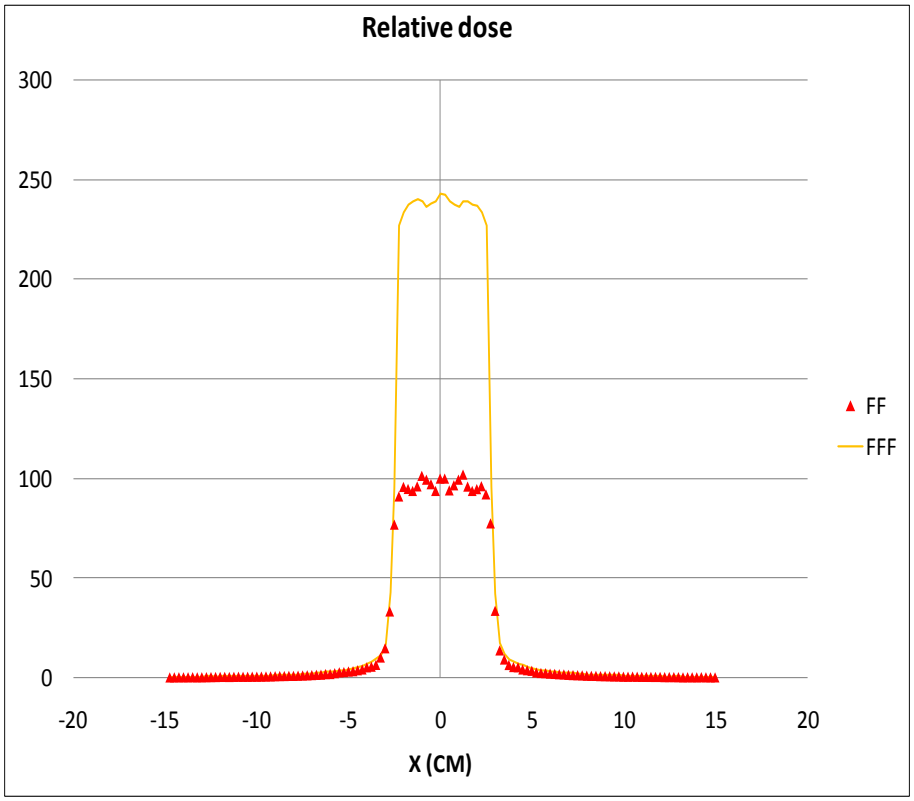

(a)

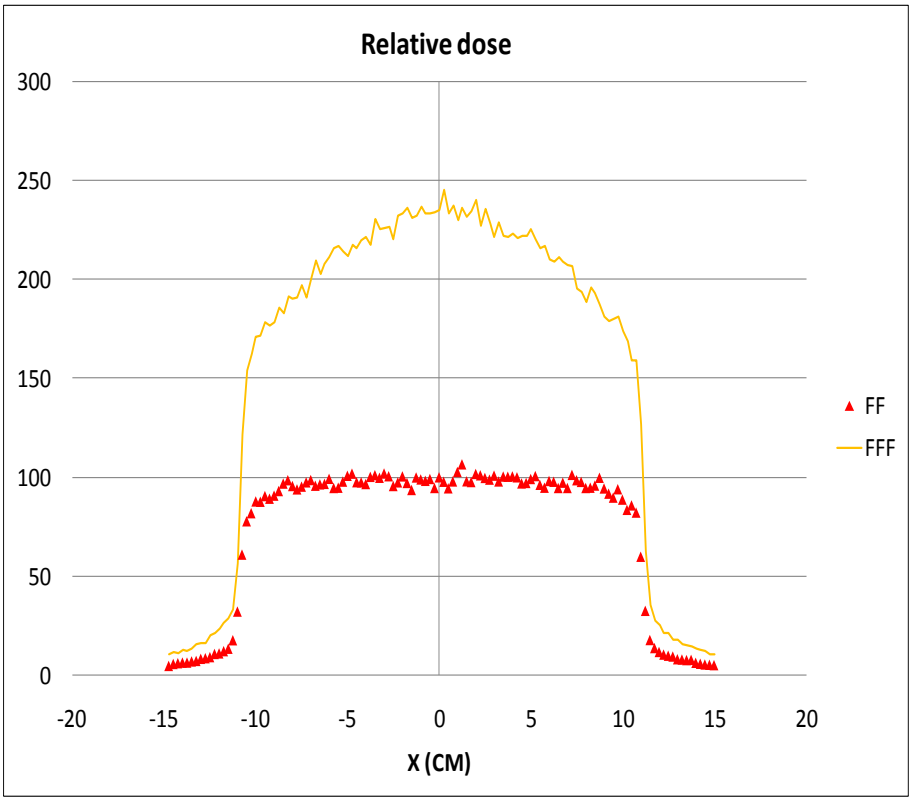

(b)

Figure. 6.2 Lateral profile for 6MV photon beams delivered with and without a flattening Filter in beam line at a depth of 10 cm for field sizes of **(a)** 5 × 5 cm^2 **(b)** 20 × 20 cm^2. Unflattened beam is normalized by the central axis dose of flattened beam. FF & FFF denotes for flattened and unflattened Beam.

6.3.1.1 Profile Normalization with Renormalization method

Lateral profiles of unflattened beams for different field sizes were calculated at 1·5 and 10 cm depth inside the water phantom. These Lateral profiles computations were carried out for both the jaw defined and MLC defined field sizes independently. To explore the possible variation in the lateral profile of unflattened beam shaped by different components of secondary collimators system we normalized them with the method described by Fogliata *et al.* to calculate their characteristics in terms of field size and penumbra at two different depths for three field sizes which are presented in Table 6.1.

Table 6.1 Unflattened 6MV photon beam profile parameters calculated for jaws only and MLC only defined field sizes. d denotes the depth inside water phantom. All Data were calculated at SSD = 100 cm.

	Field size (cm^2)					
	5×5		**10×10**		**20×20**	
	Jaw define field	**MLC define field**	**Jaw define field**	**MLC define field**	**Jaw define field**	**MLC define field**
MC calculated field size(cm)	$d=d_{max}$ 5.06 d=10 cm 5.63	$d=d_{max}$ 5.12 $d=d_{max}$ 5.75	$d=d_{max}$ 10.10 d=10 cm 11.06	$d=d_{max}$ 10.25 d=10 cm 11.20	$d=d_{max}$ 20.12 d=10 cm 22.08	$d=d_{max}$ 20.25 d =10 cm 22.25
MC calculated Penumbra (cm)	$d=d_{max}$ 0.20 d=10 cm 0.43	$d=d_{max}$ 0.23 d=10 cm 0.47	$d=d_{max}$ 0.23 d=10 cm 0.53	$d=d_{max}$ 0.31 d=10 cm 0.59	$d=d_{max}$ 0.27 d=10 cm 0.76	$d=d_{max}$ 0.35 d=10 cm 0.89

6.3.1.2 Profile Normalization with Inflection point method

In our study we computed the beam profiles for both the unflattened and flattened beam for different depths and field sizes. For comparative investigation for both kind of beams the flattened beam was normalized with central axis dose as usual while the unflattened beam in which the field size were defined either by moveable jaws or MLC were normalized using the method given by Pönisch *et al.* The comparison of lateral profiles for 20 × 20 cm^2 and 10× 10 cm^2 field sizes at a depth of 10 cm for the two cases is shown in figure 6.3 & 6.4. It was observed in our study that the unflattened beam profiles shaped by any one component of secondary collimators system had relative dose value lower than the flattened beam near the edge of measured field size. The relative decrease was found to be less for the MLC shaped unflattened beam in comparison to the corresponding jaw shaped unflattened beam. For the field size of 20×20 cm^2 measured at 9 cm off axis distance decrease in relative dose for MLC and jaw shaped unflattened beam with respect to corresponding flattened beam was found to be 12% and 15% respectively. While for a field size of 10× 10 cm^2 measured at 4 cm off axis distance reduction in relative dose for MLC shaped unflattened beam was found to be 8%.

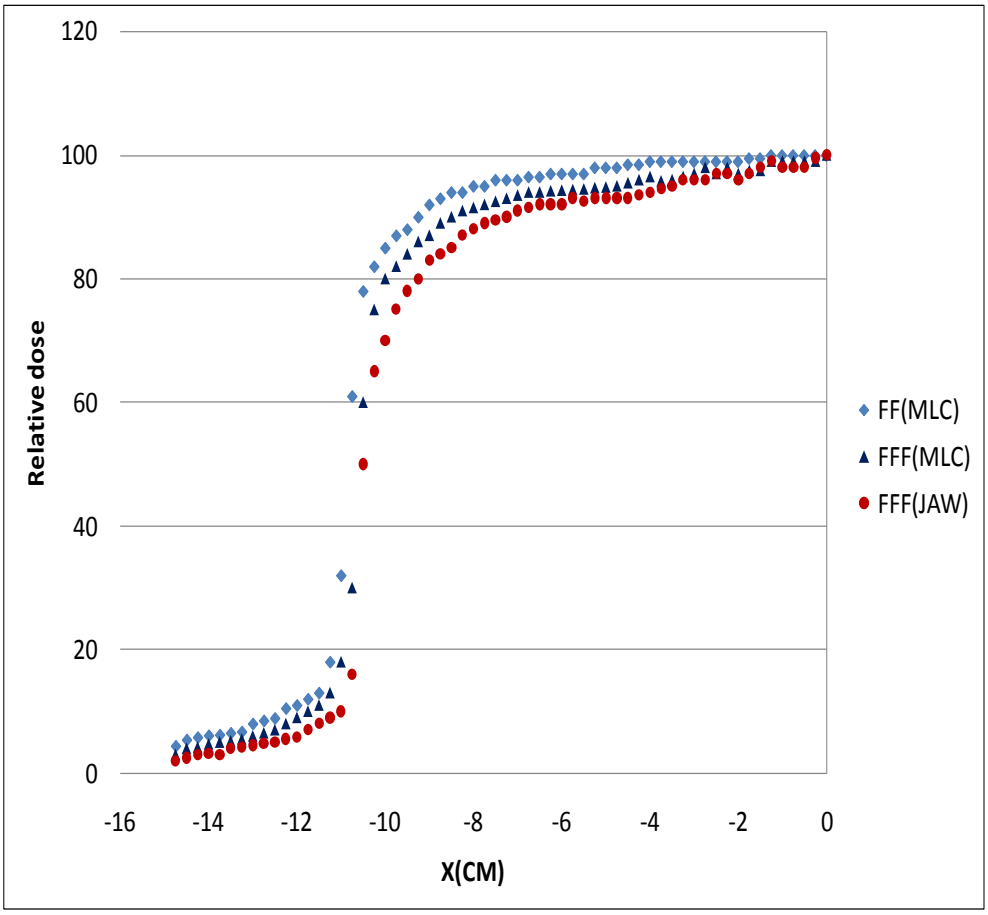

Figure. 6.3 Lateral profile comparison for 6MV photon beam for a field size of 20 × 20 cm^2 at 10 cm depth . FF (MLC) denotes flattened beam shaped by MLC, FFF (MLC) & FFF (JAW) denotes unflattened beam shaped by MLC and jaw respectively.

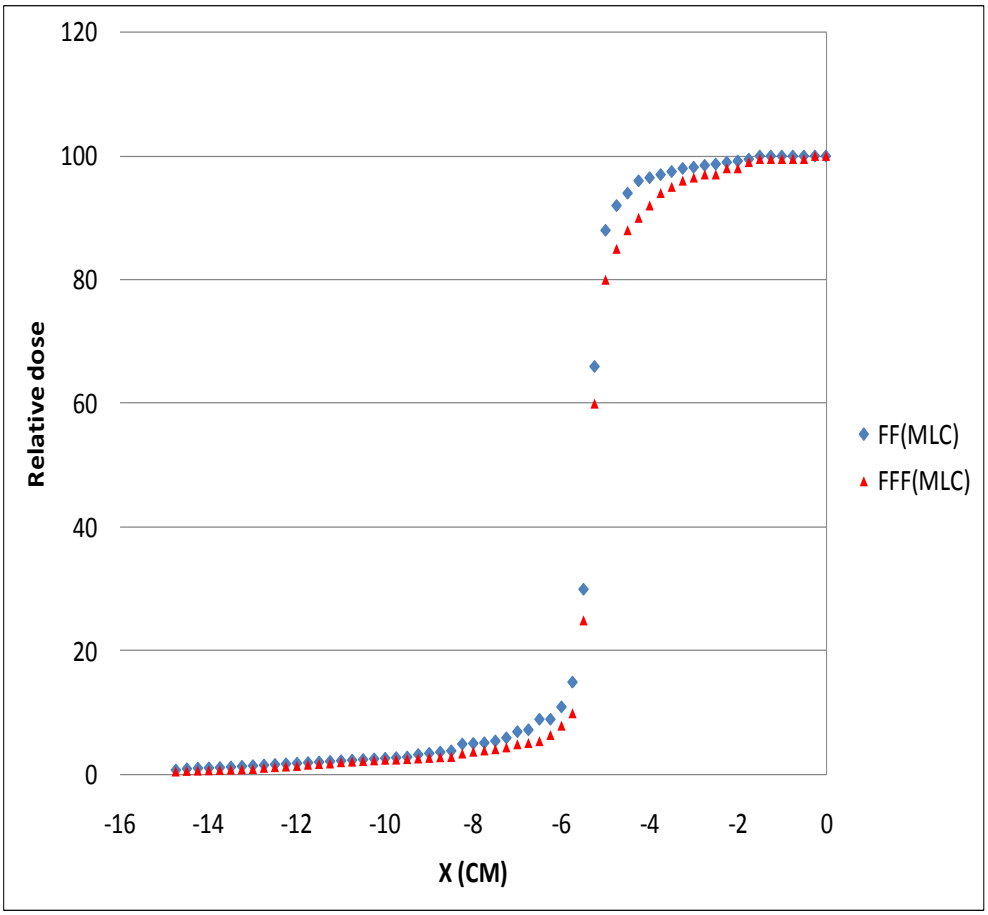

Figure. 6.4 Lateral profile comparison for 6MV photon beam for a field size of 10 × 10 cm^2 at 10 cm depth . FF (MLC) & FFF (MLC) denotes flattened and unflattened beam Shaped by MLC .

The relative dose value near the field edge region for the small field size shaped by MLC were also investigated in our study for unflattened beam and then compared with the flattened beam. Figure 6.5 shows the profiles comparison of flattened and unflattened beam for a small field size of 5 × 5 cm^2 at 5 cm depth. The relative dose at 2 cm off-axis distance is inferior in unflattened beams by 5% and it tends to decrease faster with increasing off axis distance than

it does in the flattened beams. Faster lateral dose fall-off outside the treatment field will result in lower doses to surround normal tissues.

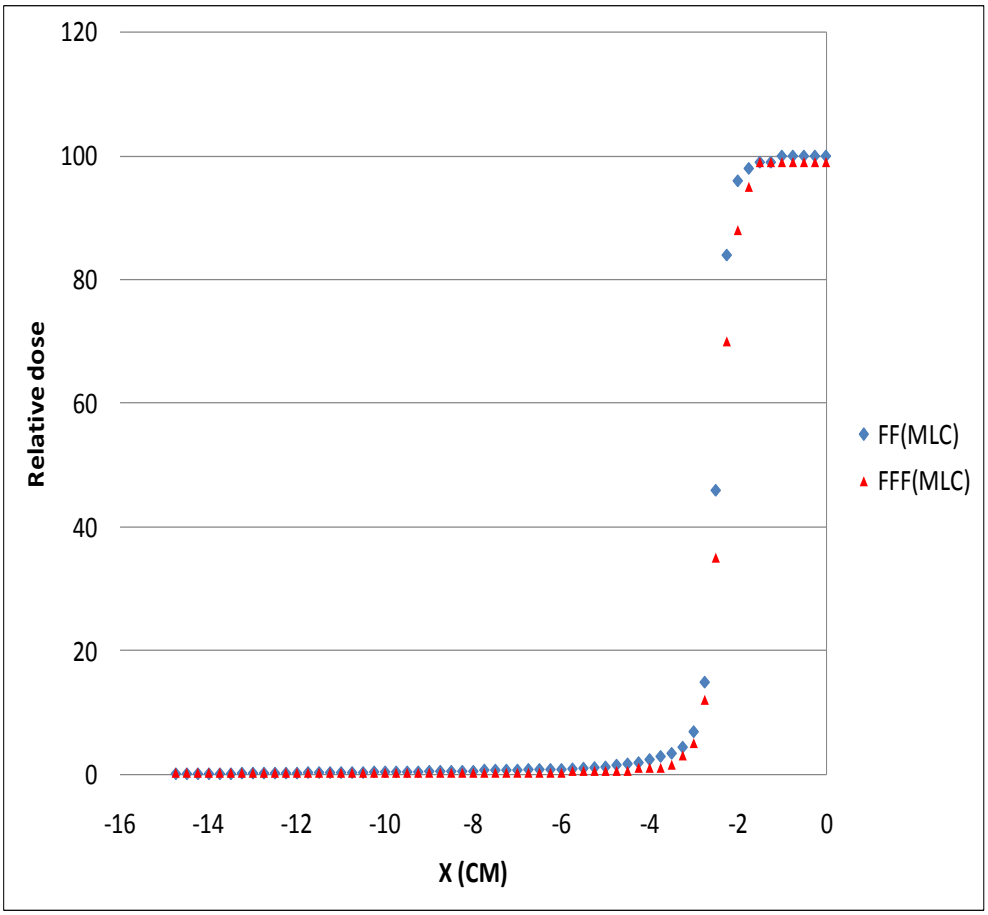

Fig. 6.5 Lateral profile comparison for 6MV photon beam for a field size of 5 × 5 cm^2 at 5 cm depth . FF (MLC) & FFF (MLC) denotes flattened and unflattened beam Shaped by MLC .

6.3.2 Analysis of spectra

6.3.2 .1 Photon fluences spectra

The photon fluence spectra was calculated at central axis by taking the scoring plain as an annular region around the central axis with radius of 2.25 cm as a function of energy (number of photons per MeV per incident electron on the target) as shown in Figure 6.6. Photons produced in the target reach the scoring plain at 100 cm SSD after passing through the

secondary collimators system in which the field size was defined by MLC for both flattened and unflattened beam. The Range of energy a photon possibly can have when it reaches the scoring is divided into equal intervals (bin) of 0·25 MeV. The number of photons within each energy interval, crossing the scoring plain was recorded for flattened and unflattened beam. The calculated central axis photon fluence spectrum was within the accuracy limit of 5% for each 0.25 MeV wide energy bin, except for the high-energy end of the spectra. Noticeable increase was observed in the photon fluence when the flattening filter was removed from the beam line.

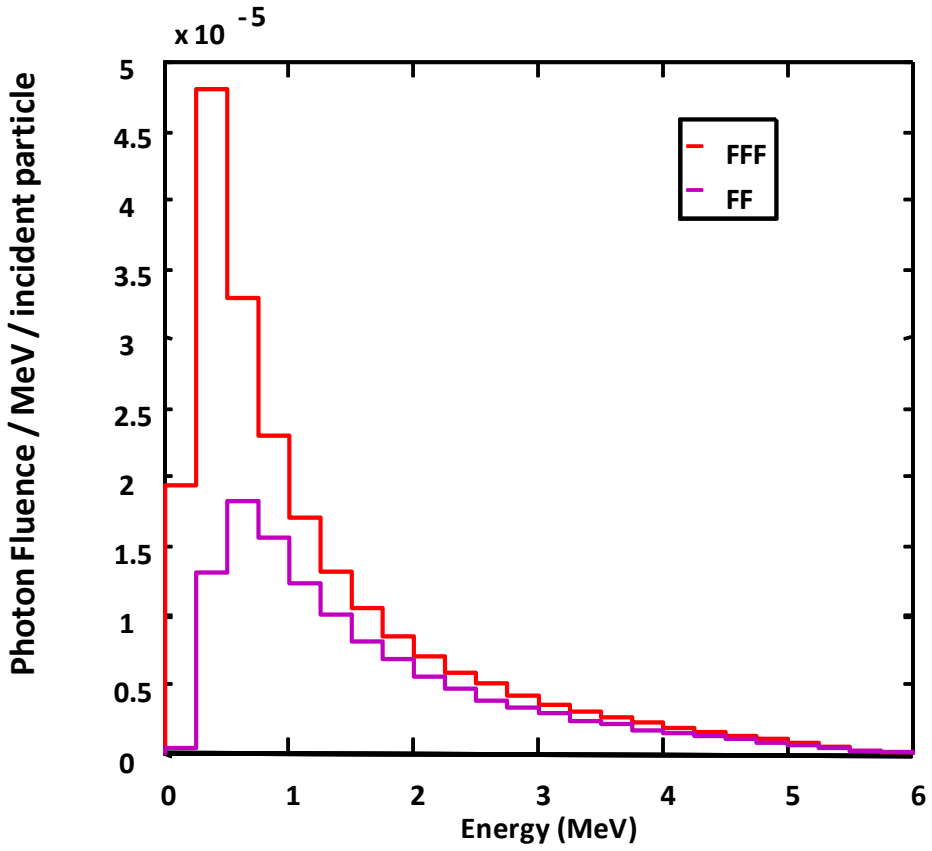

Figure 6. 6. Photon fluences per initial electron on the target, at the top of the water phantom as a function of energy (MeV) for 20 × 20 cm^2 field size calculated for with and without a flattening filter in beam line. FF and FFF denotes flattened and unflattened beams, respectively.

6.3.2 .2 Photon energy fluences spectra

Figure 6.7 represents the computed photon energy fluence spectra for large field size of 20×20 cm^2 as a function of off-axis distance in contrast to the central axis photon fluence spectra which is not energy weighted as shown in figure 6.6. After being generated in target the photon pass through the components of the Primary and secondary collimators system to reach the scoring plain at 100 cm SSD. Scoring plain was taken as an annular region around the central axis with 15 cm radius. This annular region has been divided into equal distance interval (bin) of 0.5 cm. The number of photon within each distance interval (bin) crossing the scoring plain was recorded for flattened and unflattened beams independently. The precision of calculated photon fluences spectra used for the dose calculations was very high and uncertainty in each distance interval was usually between 1 to 5%, except for the high-energy end of the spectra. A significant increase is observed in the photon energy fluence when the flattening filter was removed from the beam line on central axis and this increase tends to get minimized with increase in off-axis distance.

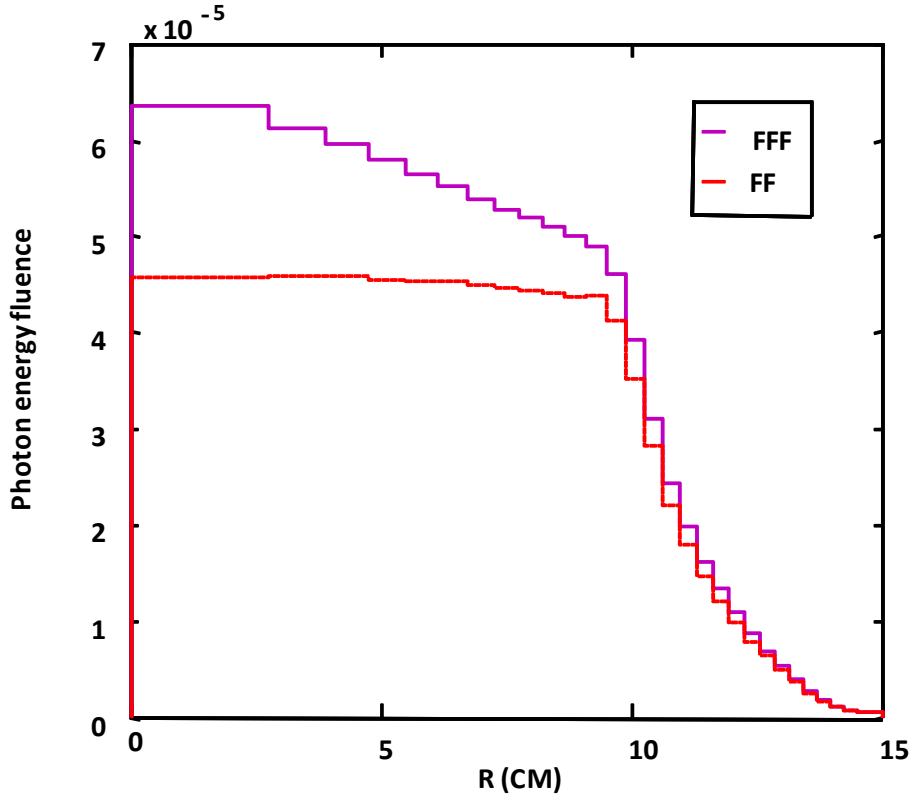

Figure.6.7 Photon energy fluences per initial electron on the target, at the top of the water

Phantom as a function of off axis distance for a field size of 20×20 cm^2 calculated for flattened and unflattened beam. FF and FFF denotes flattened and unflattened beams, respectively.

6.3.2 . 3 Average Energy Distributions

Figure 6.8 shows the average energies distribution of all the photon reaching the scoring plain as a function of off-axis distance. This distribution is calculated for a scoring plane located at SSD of 100 cm for a field size of 20×20 cm^2. In our comparative study of average energies distribution of flattened and unflattened beam it was observed that mean photon energy for flattened beam at central axis was 1·5 MeV and decreased to 1·2 MeV at off-axis distance of 20 cm. It confirmed that flattening filter produces the beam hardening effect in the filtered beam. For the unflattened beam, the mean energy of spectra was not changed significantly with increasing off-axis distance and it was, decreased from 1·25MeV on central axis to 1·19MeV at 20 cm off-axis distance for 20 ×20 cm^2 field size.

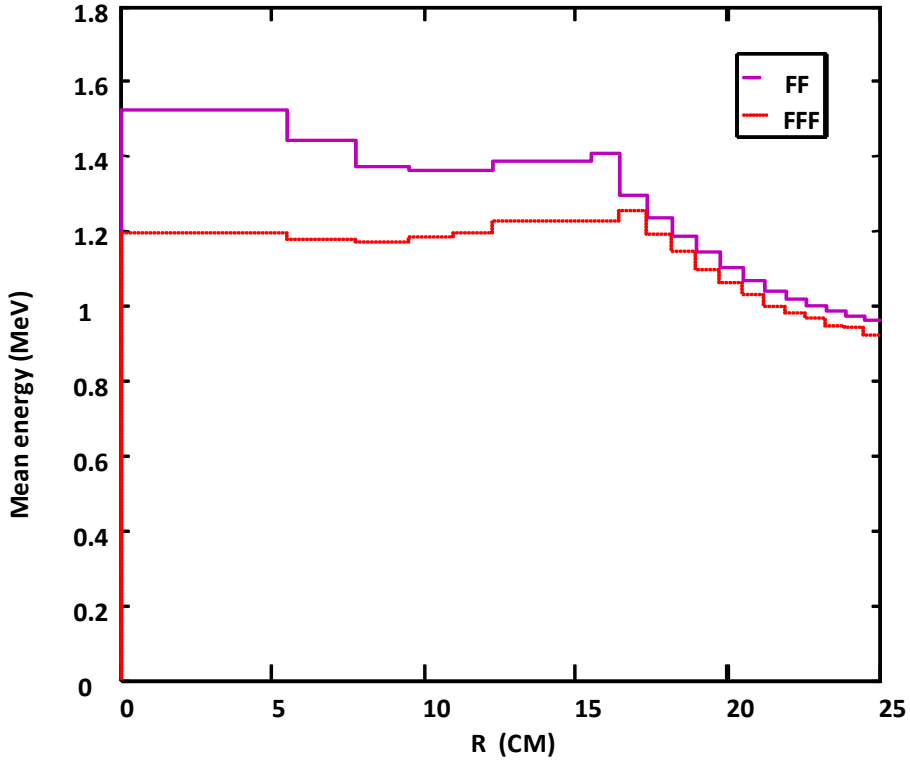

Figure 6.8 Photon average energy distribution of the filtered and unfiltered beams as a function of off-axis distance for 20 × 20 cm^2 field size and 100 cm source to surface distance. FF and FFF, flattened and unflattened beams, respectively.

6.3.2 .4 Fluence spectra of contaminant Electrons

Increase in electron fluence on central axis may affect the accuracy of measurement system used for the dosimetric calculation as they consist of ion chamber which has limited range of its reliable operation. In addition due to low energy of these undesirable particles, they contribute in skin dose delivered by radiation beam. Thus for these reasons we found essential to investigate the effect of flattening filter on electron fluence spectra delivered by the radiation beam. Figure 6.9 shows the fluence spectra of electrons calculated at central axis with a radius of 2.5 cm and the possible range of energy electron can achieve is being divided into equal energy interval (bin) of 0·25MeV for both flattened and unflattened beam.

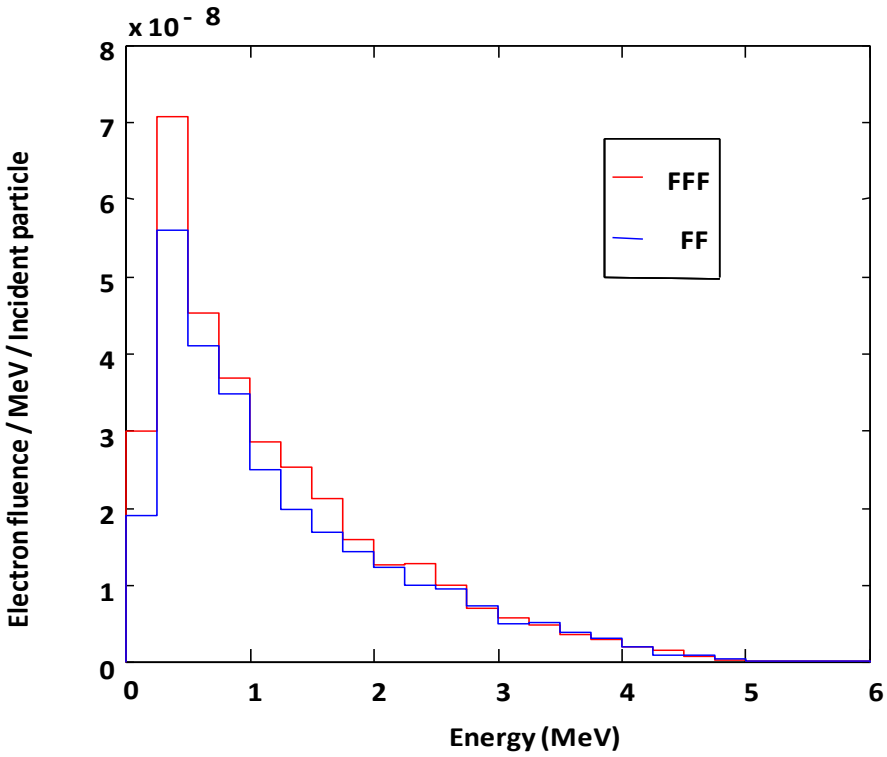

Figure 6.9 Electron fluences spectra per initial electron on target, at the top of the water phantom as a function of energy for a field size of 20×20 cm^2 for both flattened and unflattened beam . FF and FFF denotes the flattened and unflattened beams, respectively.

6.3.2 .5 Energy fluence spectra for Electron

The energy fluence spectrum of electron for the both kinds of beam is shown in figure 6.9. It shows the variation for the central axis only and do not provide any information of electron fluence variation with increase in off-axis distance. To evaluate the effect of removing the flattening filter from beam line on electron fluence as a function of off-axis distance we computed energy fluence spectra of electron as a function of off-axis distance for the unflattened and flattened beam which is presented in figure 6.10. Numbers of electron reaching the phantom surface were found to increases with removing the flattening filter from the beam line. However, the difference close to the central axis is higher and tends to decreases as the off axis distances increases for the two kinds of beams. Monte carlo calculation demonstrated that the electron fluence at central axis for a 6 MV flattening filter

free beam was 1.2 times greater than its value for with flattening filter for a field size of 20×20 cm^2.

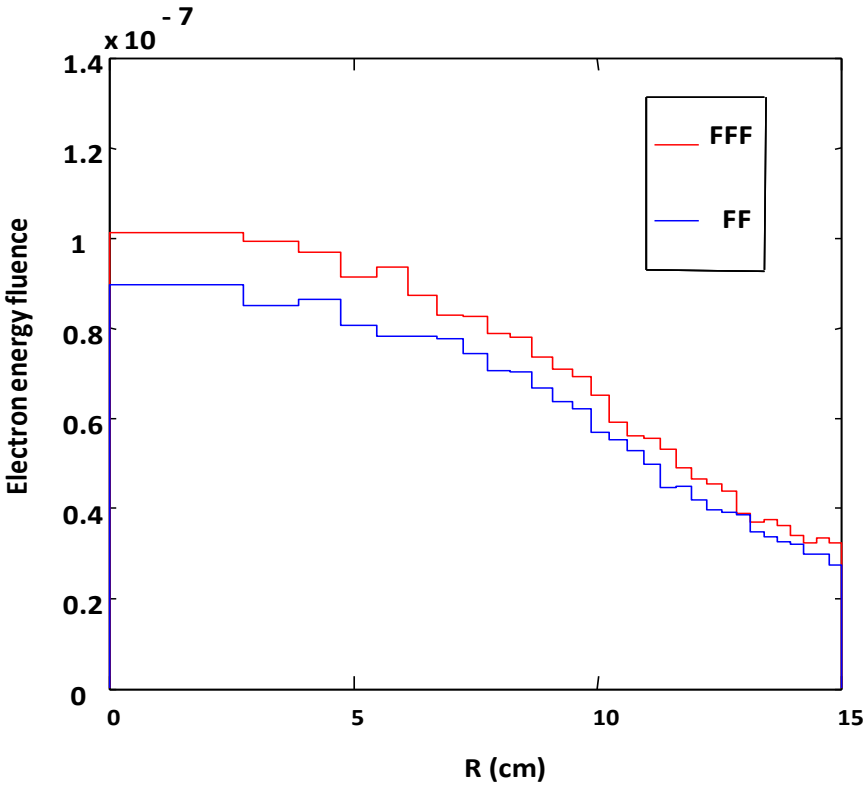

Figure.6.10 Electron energy fluences per initial electron on target, at the top of the water phantom as a function of off axis distance calculated for a field size of 20×20 cm^2 . FF and FFF, flattened and unflattened beams, respectively.

6.3.3 Depth dose profile analysis

6.3.3 .1 Absolute dose

In our study of unflattened beam depth dose profile on central axis, we computed the absolute absorbed dose per initial electron on target for both the flattened and unflattened beam for different field sizes and at two reference depths of 1.5 and 10 cm. The field sizes for the above computation were defined with MLC for both kinds of beams. Absolute depth doses ratio calculated for flattening filter free to standard flattened beams is presented in table 6.2. The computed Absolute depth doses ratio suggest a significant increase in absolute absorbed dose when flattening filter is removed from the beam line, indicating an increase in dose rate

for unflattened beam. However, this increase in dose rate tends to decrease with increase in depth.

Table 6.2 Ratios of absolute depth doses for unflattened to flattened beams at two references depths for different field sizes. A denotes the field size; d denotes the depth inside water phantom. Absorbed dose calculated without the flattening filter in the beam line is denoted as D_{FFF} (flattening filter free) and with filter in beam line is denoted as $D_{FF.}$

A(cm^2)	$\left(\frac{D_{FFF}}{D_{FF}}\right)$**At d=1.5**	$\left(\frac{D_{FFF}}{D_{FF}}\right)$ **At d=10**
5×5	2.49	2.42
10×10	2.47	2.45
20×20	2.44	2.40

6.3.3.2 Percentage depth-dose characteristics

Absolute depth dose values were used to generate percentage depth-dose **(**PDD) curves for the flattened and unflattened beam. It was observed from the comparison of PDDs of both beam that unflattened beam tends to have relatively inferior value compared to the corresponding flattened beam for all field sizes studied in this investigation (as shown in figure 6.11). The difference in the relative dose value presented by the PDDs of two kind of beam was more apparent at deeper depths and increased with increase in depth. To quantify these differences two parameters are calculated and reported in Table 6.3, namely, the relative dose at a depth of 10 and 20 cm (D_{10}, D_{20}).

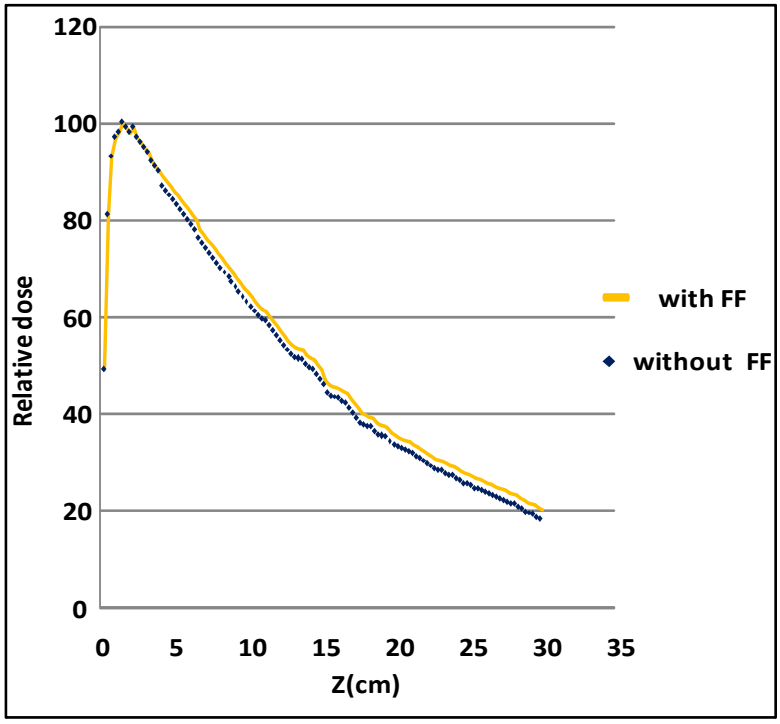

(a)

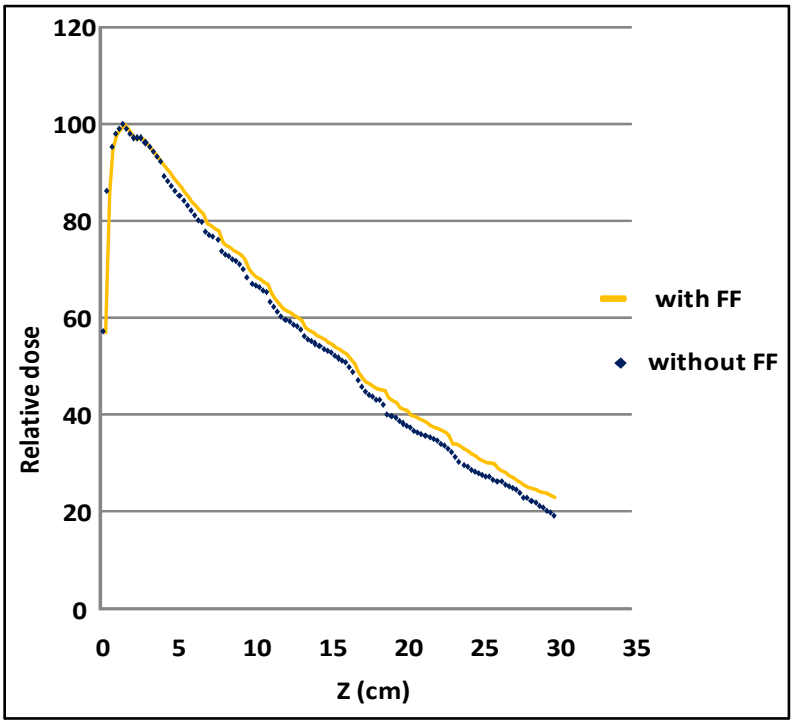

(b)

Figure. 6.11 Comparison of relative depth dose curves calculated for with and without flattening filter for field sizes of (a)10×10 cm^2 (b) 20×20 cm^2
Abbreviations: FF denotes flattening filter

Table 6.3 Relative depth doses Comparison of flattened and unflattened beams at two reference depths for different field sizes. A denotes the field size; D_{10} and D_{20} denotes relative depth dose at 10 and 20 cm depth; FF denotes flattening filter.

A(cm^2)	Relative dose at depth of 10 cm D_{10}		Relative dose at depth of 20 cm D_{20}	
	With FF	**Without FF**	**With FF**	**Without FF**
5×5	62.43	59.40	33.26	30.84
10×10	66.70	63.80	37.80	34.34
20×20	71.65	68.96	40.98	37.55

6.3.4 MLC Leakage

A vital parameter required for the commissioning of any morden treatment-planning system is MLC leakage. In our study we computed the MLC leakage as a function of field size for the unflattened beam and presented in Table 6.4. MLC leakage represents the dose on central axis with MLC blocked fields normalized by the dose for open fields of the same field size at 1.5 cm depth for 100 cm SSD. Open field are define by the X & Y treatment jaws only. MLC blocked fields define a field in which the MLC leaves are configured to fully block the open field produced by the jaws. To ensure that the jaws blocked the rounded tips of the leaves completely in MLC blocked fields, the leaves of MLC were positioned asymmetrically with respect to the central axis and there projected offset at isocenter was 8.0 cm.

Table 6.4 MLC leakage calculated for 6 MV photon beam deliver with or without flattening Filter in beam line for different field sizes. all calculations were made at 1.5 cm depth and SSD of 100 cm.

	MLC leakage	
Field size (cm^2)	**With flattening filter**	**Without flattening filter**
5×5	-	1.10
10×10	1.40	1.23
20×20	-	1.32

6.3.5 Scatter function

The total scatter factor, S_{CP} is defined as 'the dose rate at a reference depth for a given field size divided by the dose rate at the same point and depth for the reference field size (10 × 10 cm^2). It was measured at SSD = 100 cm and a depth equal to d_{max} of a 10 × 10 cm^2 field for different field sizes. We computed the total scatter factor for three types of beams; flattened beam delivered with field size defined by MLC, unflattened beam delivered in which field size were defined by either MLC or movable jaws only. The data for all three kinds of beams is presented in Table 6.5.

Table 6.5 Total scatter factor Scp calculated for 6 MV photon beams delivered with three different modes. The Scp was measured at SSD = 100 cm, and at the depth of maximum dose d_{max} of a 10 × 10 cm^2 field size.

Field size (cm^2)	**Scp (MLC shaped) (with FF)**	**Scp (JAW shaped) (without FF)**	**Scp (MLC shaped) (without FF)**
5×5	0.967	0.97	0.98
10×10	1	1	1
15×15	1.021	1.012	1.010
20×20	1.054	1.027	1.018

6.4 Discussion & Conclusion

In this chapter our investigation was focused upon evaluating the differences in the dosimetric characteristics of unflattened beam shaped by either MLC or movable jaws and furthermore we carried out there comparison with the corresponding flattened beam. To accomplish this job, we performed Monte Carlo simulations for computation of lateral profiles for different modes of delivery of radiation beam. Lateral beam profiles thus calculated for unflattened beam were normalized using different methods. First we used the method described by Fogliata *et al*. to normalize the unflattened beam shaped by ether jaws or MLC so that there characteristics could be compared with the flattened beam. It was observed in our study that the dosimetric field size was somewhat inferior for unflattened

beam compared to flattened beam; however, the amount of decrease in field size was less for MLC shaped then it was with jaw-shaped unflattened beam. The maximum difference in MLC and jaw shaped unflattened beam field size was 1·7mm which was obtained for 20× 20 cm^2 field size measured at 10 cm depth. It was even less for the smaller field sizes measured at different depths. The penumbra calculated for lateral profiles of unflattened beam were also found to be smaller than the flattened beam. Though the differences in penumbra values for unflattened beam shaped by MLC and jaw were small with the maximum value of 1·3 mm. This difference may not appear large, but is significant in modern radiation treatments. We proceeded in our comparative investigation of the two kind of beam by using the method given by Pönisch *et al.* for the normalization of unflattened beam delivered with differ settings of secondary collimator system. The lateral profiles of unflattened beam after normalization when compared to the analogous flattened beam were found to have lower relative dose value in the near field edge region and additionally showed faster rate of decline with increase in off-axis distance. In this comparison again the decline in MLC shaped unflattened beam was less than the jaw shaped unflattened beam. This behaviour of unflattened beam could be illustrated as; removing the filter cause decrease in the scattering of primary photons and decreases the relative fluence of primary photons propagating towards off-axis. These results are alike to those which were obtained when the unflattened beam was normalized with the method described by Fogliata *et al*, thus increasing the trustworthiness of our simulation study.

In our investigation we evaluated central axis depth dose profile for both the flattened and unflattened beam shaped by MLC. The major portion of primary photons generated in the target passes through the flattening filter which presents substantial quantity of material in their path through which they have to pass through before reaching the scoring plane to deliver dose. This major halt present in the path of primary photons removes large portion of

them and also introduces scattering. Thus removing the filter from the beam path should result in decrease in beam-on time and out-of-field exposure of patients experiencing the radiation treatment. We computed absolute absorbed dose per initial electron incident on target for both flattened and unflattened beam for different field sizes at two reference depths. The ratio of absolute depth doses for unflattened beam to standard flattened beams for a standard field size of 10×10 cm^2, at 10cm depth for an 100 cm SSD was found to be 2·45 indicative of the potential higher dose rate deliver by the unflattened beam. Unflattened beam was found to have slightly lower PDDs value when compared with the standard flattened beam for all the field sizes investigated in our study. Difference in the PDDs of flattened and unflattened beams were more obvious at deeper depths and increased with increase in depth.

To authenticate the results derived from the ratio of absolute depth doses for the two kind of beam shaped by MLC we evaluated the spectral characteristics of photons which are responsible for majority of dose delivered by the radiation beam. We computed the variation of photon fluence with energy delivered by radiation beam which showed that the averaged value of photon fluence on central axis calculated over the total surface of top of water phantom increased drastically which was primarily responsible for the increased dose rate of unflattened beam. Fluence spectra variation with off-axis distance for photons showed similar results on central axis but with increase in off-axis distance the increment in fluence of photons for unflattened beam tends to get diminished.

Furthermore we computed the average energy variations of photons as a function of off-axis distance as a part of our study of spectral characteristics of unflattened beam and subsequently compared them with those of the flattened beam. It was observed that for the unflattened beam the mean energy of photon energy spectrum reduced from 1.5 to 1.25 MeV on the central axis calculated for a large field size of 20 × 20 cm^2. The flattened beam mean

energy showed more deviations with increase in off-axis distance as it decreased from 1·5MeV on central axis to 1·2MeV at off-axis distance of 20 cm, whereas no such large variation in average energy was observed for the unflattened beam. The mean energy of photons of unflattened beam showed small variations as it decreased from 1·25MeV on central axis to 1·19MeV at 20 cm off-axis distance . The flattening filters used in medical linear accelerators are conical in shape with their central part to be thicker and this thickness tends to decrease near the sides of the filter. The central part of the filter presents more attenuation to the primary photons and eliminates the possible low energy components present in it, thus filter elevates the mean energy of photons on central axis. As the off-axis distance from the central axis increases the thickness of filter decreases allowing these low energy components to pass through it and contribute in the average energy thus lowering its value. Therefore, the flattened beam shows more variation in mean energy with increase in off-axis distance then the corresponding unflattened beam.

MLC leakage is a very important factor in any morden treatment as it represents the amount of undesired dose delivered due to leakage through the MLC which are supposed to have no leakage once configured to block any portion of treatment field. Therefore we investigated the effect of flattening filter on MLC leakage. We observed in our calculation of this parameter for both the flattened and unflattened beam that there was a substantial decrease in MLC leakage when the flattening filter was removed from the beam line, as for 10×10 cm^2 field size its value was 1·4 which decreased to 1·23 with filter removed from the beam line. The possible explanation for this decrease in MLC leakage is due to the differences in the average energy distributions of the two kind of beam. As we discussed above the flattened beam have relatively higher mean energy of photons due to which less amount of attenuation take place, while in the absence of filter more low energy particle contribute in unflattened beam leading to increased attenuation of it by the MLC.

To examine the effect of flattening filter on head scattered radiation we computed the total scatter factor, S_{CP} for both unflattened and flattened beam. Our calculated data showed a sluggish variation of S_{CP} with increase in field size for unflattened beam in comparison to the flattened beam which is very understandable since the filter is the major source of scattering of primary beam. Additionally, our data showed that the amount of variation in S_{CP} was even less for MLC shaped unflattened beam in comparison to jaw-shaped unflattened beam, which suggest that use of MLC to define field size offers advantage over jaw for unflattened beam in terms of more reduced scatter radiation. Finally from all above comparative study we conclude that apart from the advantages of unflattened beam over flattened beam, use of multileaf collimators to define the treatment field size for unflattened beam will provide enhanced accelerator characteristics.